Chapter 9
Analytical Models for Axially-Restrained Steel–Concrete-Steel Sandwich Panel Under Blast

9.1 Introduction

Steel–Concrete-Steel (SCS) sandwich panels were demonstrated to have good blast resistant performances through field blast tests (Liew and Wang 2011; Lan et al. 2005), and therefore they could be employed as protective structures against impact and blast loads. Previous studies showed that the SCS sandwich panel with axially-restrained boundary had significantly higher blast resistance as compared to its counterpart with simply supported boundary. Hence, the aim of this study is to develop the analytical models for predicting axially-restrained SCS sandwich panels under blast loading.

For a simply supported SCS sandwich panel, its failure mode includes flexure and shear. Therefore, the mechanical shear connectors are of significance to assure the composite action of SCS sandwich panels. Liew and Sohel (2009) proposed J-hooks and studied the impact performances of SCS sandwich beams with J-hook connectors (Liew et al. 2009). Moreover, field blast tests were also conducted to obtain the blast responses of SCS sandwich panels with J-hook connectors (Liew and Wang 2011). For the axially-restrained SCS sandwich panels, it mainly relies on the tensile membrane action to resist lateral pressure load, and therefore the shear connectors are relatively unimportant. Remennikov and Kong (2012) carried out the impact tests on the axially-restrained non-composite SCS sandwich panels. The tensile membrane resistance was found to be significantly higher than the bending resistance, and the ductility of the SCS sandwich panel was also improved (Remennikov and Kong 2012; Remennikov et al. 2013). The membrane action of Reinforced Concrete (RC) panels has already been considered in fire resistance design when the RC panels undergo large deformation after fire (Li et al. 2007; Bailey 2001). The formula used to predict resistance of RC panels considering membrane action was generally derived based on force equilibrium. The resistance–deflection function is necessary to predict the structural response under dynamic loading. In this study, the resistance–deflection function of the SCS sandwich panel contributed by concrete core is derived based

Y. Wang et al., *Innovations in Impact and Blast Protections*,
https://doi.org/10.1007/978-981-19-4375-1_9

on the energy balance principle, since the force distribution on the concrete core is complex and it is nearly impossible to establish the force equilibrium equations.

The Single-Degree-Of-Freedom (SDOF) method is commonly adopted to predict the structural response under blast loading (UFC 2008; Biggs 1964; ASCE 2011), as it is a relatively simpler alternative as compared to the Finite Element (FE) method and the calculations are reasonable in most cases. A structural member can be equivalent to a SDOF system through transformation factor K_{LM}, which is a function of its deflection shape (Biggs 1964). Normally, the shape function is obtained by analyzing the member under uniformly distributed static load. In reality, the deflection shape changes during motion owing to the existence of inertia force which, together with the uniform pressure load, changes the load distribution on the member. It is accepted that shape function has little effect on the structural response if the adopted deflection shapes are in accordance with the actual boundary condition. However, the difference in maximum displacement obtained using different assumed shape functions may be over 10% in the elastic range (Baker et al. 1983) and may be even larger when the member enters plastic range. A constant value of Dynamic Increase Factor (DIF) was generally included in the SDOF model to represent the average strain rate effect on material strength (UFC 2008; ASCE 2011). Since the DIF is a function of strain rate, it also varies during motion. Hence, adopting a constant value of DIF may not accurately capture the strain rate effect. To overcome this limitation, Nassr et al. (2012) proposed a strain rate model that defines the maximum strain rate in terms of scaled distance for beam column. Different DIF values can be generated under different blast loads, but the model is still unable to capture the varying DIF with strain rate during motion. The varying DIF in terms of strain rate was recently included in the continuous beam model (Carta and Stochino 2013; Jones et al. 2009) and SDOF model (Carta and Stochino 2013) to analyze the simply supported RC panels under blast loading. The DIF was introduced by updating the resistance at each time step according to the strain rate at the corresponding time step, and the predictions with varying DIF were more accurate than those with constant DIF by comparing with test results.

In this chapter, the resistance–deflection function of the axially-restrained SCS sandwich panel was derived and then included into the SDOF model. The varying DIF in terms of strain rate was also considered in the SDOF model. Since only one deflection shape function can be included in the SDOF model, the Lagrange Equation model (Donaldson 2006; Schleyer and Hsu 2000; Langdon and Schleyer 2005) with combined shape functions and varying DIF was introduced to better predict the blast responses of axially-restrained SCS sandwich panels.

9.2 FE Model Calibration

9.2.1 Blast Loading Test on SCS Sandwich Panels

The field blast tests on SCS sandwich panels conducted by Kang et al. (2013) were employed for the FE model validation. There were six specimens being fabricated for three blast tests, and two specimens were tested in each blast test. The 100 kg TNT military cratering ordnance was detonated at a standoff distance of 5 m (Liew and Wang 2011; Kang et al. 2013). The setup of field blast test is shown in Fig. 9.1. Although six specimens were tested, only one specimen with normal concrete and without shear connectors was selected for validating the established FE model in the following section. The configuration of the non-composite SCS sandwich panel with normal concrete is shown in Fig. 9.2.

9.2.2 FE Model Establishment

The FE model of the SCS sandwich panel is shown in Fig. 9.3. Thick-shell and solid elements are used to mesh the steel plates and concrete core, respectively. The front, back, side and end steel plates were fillet welded together to form the outer skins of the panel during fabrication. Since no weld failure was observed after the blast test, the perfect weld condition is employed in the FE model by merging the coincident nodes of steel plates.

The Continuous Surface Cap (CSC) model in LS-DYNA (Hallquist 2006) was adopted to simulate the behavior of concrete. The CSC model was developed by US

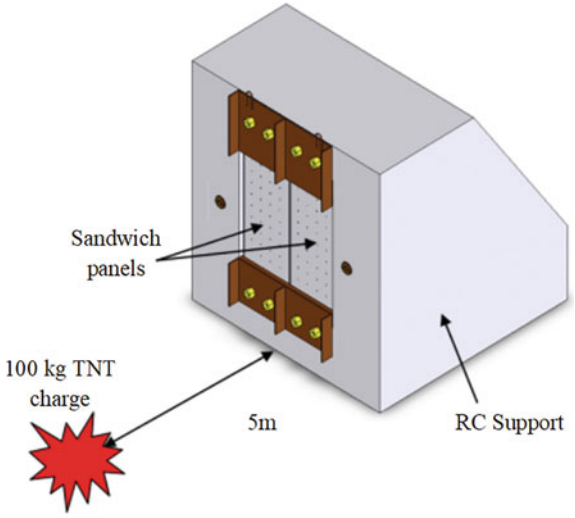

Fig. 9.1 Blast test setup with 100 kg TNT charge (Kang et al. 2013)

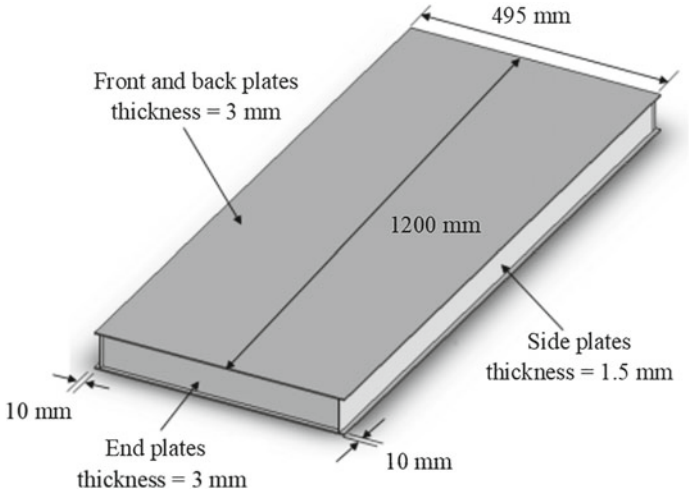

Fig. 9.2 Details of SCS sandwich panel (Kang et al. 2013)

Federal Highway Administration for simulating the concrete-like material subjected to impact and blast loads (FHWA 2007a, b). This model has been proven to be a robust constitutive model for both implicit and explicit analysis. The detailed introduction of failure surface, flow rule, damage formulation and strain rate treatment for the CSC model can be found from FHWA (2007b). This FHWA material model is easy to use, since it can generate the default parameters for the normal concrete by only inputting the unconfined compressive strength. The main material parameters of concrete used in this analysis are given in Table 9.1.

Piecewise Linear Plasticity (PLP) model in LS-DYNA was adopted for the steel material. The input true stress–effective plastic strain curve was obtained from the tensile coupon test results. Cowper-Symonds equation (Cowper and Symonds 1958) is included in this material model to consider the strain rate effect, as shown in Eq. (9.1).

$$DIF_s = 1 + \left(\dot{\varepsilon} / c\right)^{1/p} \tag{9.1}$$

where c and p are strain rate parameters. For mild steel, the values of c and p are taken as 40.4 s^{-1} and 5, respectively (Jones 1988).

9.2.3 FE Model Validation

The blast pressure–time history recorded in the test is plotted in Fig. 9.4, together with the integrated impulse. The equivalent triangular blast load with similar peak

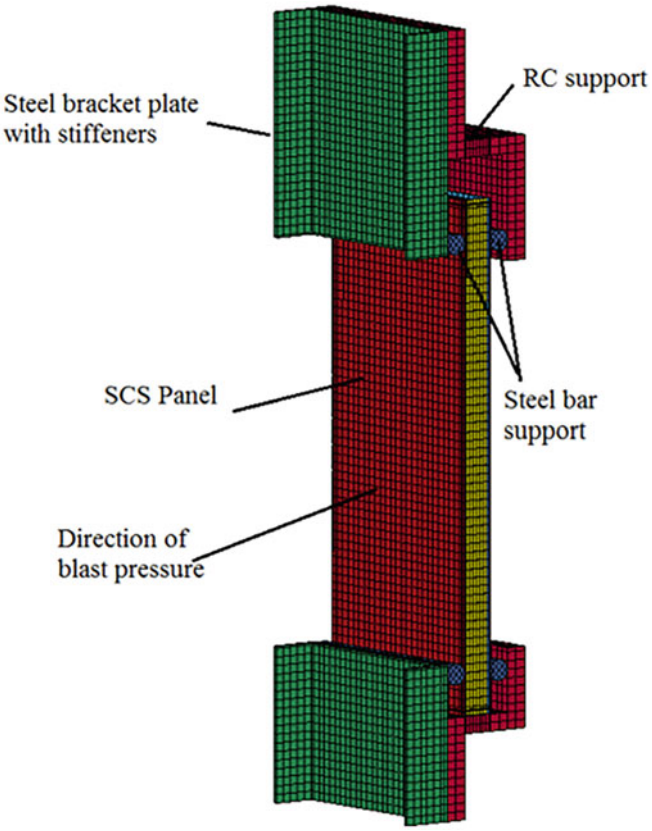

Fig. 9.3 FE model of SCS sandwich panel and support, reprinted from Wang et al. (2015), copyright 2022, with permission from Elsevier

Table 9.1 Material properties of concrete in FE analysis

Density (kg/m^3)	Compressive strength (MPa)	Shear modulus (GPa)	Bulk modulus (GPa)
2310	35	12.06	13.21

impulse and pressure is applied in the FE model, as shown in Fig. 9.4. The mid-span permanent displacement of the SCS sandwich panel from blast test is compared with the FE-prediction, as shown in Fig. 9.5. Since the potentiometers failed to capture the data during the field blast test, the displacement–time history was not compared. Figure 9.5 shows that the measured permanent displacement from the blast test agrees well with the FE-prediction. Moreover, the FE-predicted failure mode of the SCS sandwich panel is also compared with test observations in Fig. 9.6. Both FE and test results exhibit the flexural failure mode at mid-span, with sign of shear deformation at

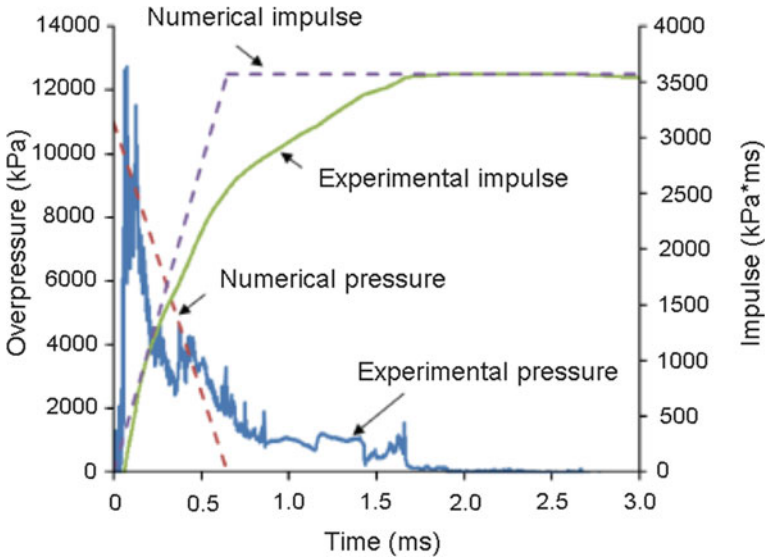

Fig. 9.4 Experimental and numerical blast loading profiles (Kang et al. 2013)

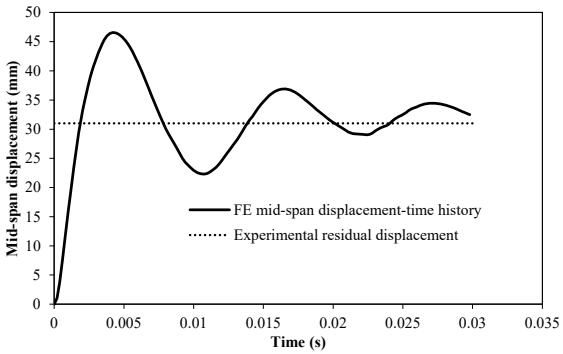

Fig. 9.5 Comparison of experimental and numerical results, reprinted from Wang et al. (2015), copyright 2022, with permission from Elsevier

the top end. Therefore, the established FE model can produce reasonable predictions on the responses of SCS sandwich panels subjected to blast loading. The established FE model will be used to verify the analytical models in the following sections by removing the side plates and support as well as imposing the axially-restrained boundary.

Fig. 9.6 Comparison of failure modes from **a** blast test and **b** numerical simulation, reprinted from Wang et al. (2015), copyright 2022, with permission from Elsevier

9.3 SDOF Model

The SCS sandwich panel can be equivalent to a SDOF system, and the deflection shape function and resistance–deflection function of the SCS sandwich panel are necessary to establish the equation of motion as

$$K_{LM} m \ddot{y} + R(y) = F(t) \tag{9.2}$$

where K_{LM} is the load-mass factor and can be calculated based on the given deflection shape function; $R(y)$ is the resistance–deflection function.

The deflection shape function and resistance–deflection function are generally derived by solving the differential equations established according to the force equilibrium. However, it is hard to establish the force equilibrium equations for the SCS sandwich panel owing to the undetermined composite action between steel plates and concrete core as well as the complex stress–strain relationship of concrete. In this study, the resistance–deflection function of the SCS sandwich panel is divided into two parts, i.e., the resistance contributed by steel plates and concrete core. The resistance–deflection function of the axially-restrained steel plate considering tensile membrane action has been obtained by utilizing force equilibrium equation (Wang and Xiong 2015), which is given as

$$R_s(Y) = \begin{cases} \dfrac{21.104 E t_s Y^3}{L^4} & \varepsilon \le \varepsilon_y \\ \dfrac{8 E t_s \varepsilon_y (1-\alpha) Y}{L^2} + \dfrac{21.104 \alpha E t_s Y^3}{L^4} & \varepsilon > \varepsilon_y \end{cases} \tag{9.3}$$

where E is the Young's modulus, t_s is the steel plate thickness, Y is the mid-span displacement, L is the span length, ε_y is the yield strain, and α is the steel hardening coefficient. The deflection shape function has been obtained as (Wang and Xiong 2015)

$$\phi(x) = \frac{4}{L^2}(Lx - x^2) \tag{9.4}$$

The deflection shape function of the steel plate in Eq. (9.4) is also adopted as the deflection shape function for the SCS sandwich panel. This is because the deflection shape function has little effect on the structural response (Baker et al. 1983), and the steel plates of the SCS sandwich panel absorb the majority of blast energy. Another reason is that the constant curvature along the span of the SCS sandwich panel can be obtained according to the shape function in Eq. (9.4), which will significantly simplify the calculation.

The energy balance principle is adopted to derive the resistance–deflection function of the SCS sandwich panel contributed by concrete core. The procedure is that: (a) obtaining the strain distribution of concrete core and establish the relationship between strain and mid-span displacement; (b) deriving the relationship between the internal energy of concrete core and mid-span displacement; (c) differentiating the internal energy with respect to mid-span displacement and divided by load factor K_L to obtain the resistance–deflection function of the SCS sandwich panel contributed by concrete core.

9.3.1 *Resistance–Deflection Function Contributed by Concrete Core*

To simplify the calculation of resistance–deflection function of the SCS sandwich panel contributed by concrete core, the following influences are ignored, i.e., the tensile strength of concrete, the confinement effect on compressive strength of concrete, and the bonding and friction between steel plates and concrete core. Then, the force distribution on the concrete core and the compression strut along the span can be given in Fig. 9.7, together with the neutral axis along the span. According to the force equilibrium in horizontal direction, the compressive force from the end plate equals to the compressive force in concrete, i.e., $F_e = F_c$. Therefore, it is reasonable to assume that the neutral depth (the distance between the outmost compression layer and neutral axis) at the end and mid-span is the same. Hence, according to Fig. 9.8, t_1 equals to t_2, which leads to the following relationship.

$$\frac{\Delta L_S}{t_n - t_1} = \frac{\Delta L_C}{t_2} \tag{9.5}$$

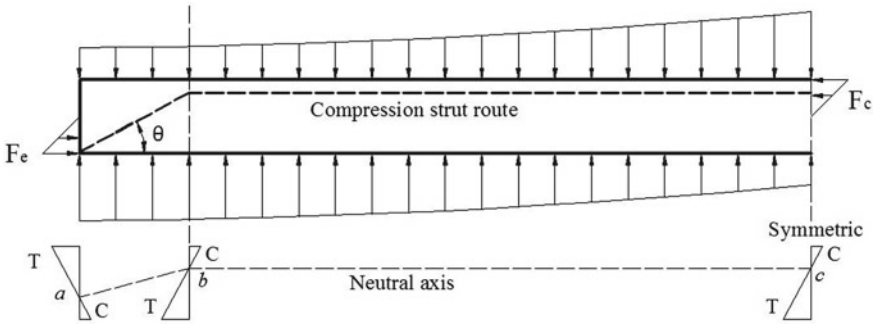

Fig. 9.7 Force distribution and neutral axis on the concrete core, reprinted from Wang et al. (2015), copyright 2022, with permission from Elsevier

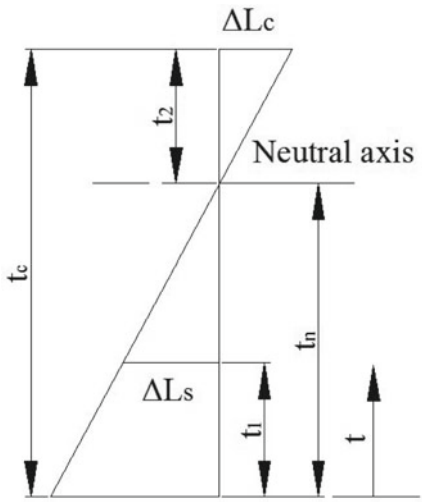

Fig. 9.8 Deformation profile across the concrete depth, reprinted from Wang et al. (2015), copyright 2022, with permission from Elsevier

where ΔL_S is the difference between developed length and original length of the steel plate, and ΔL_C is the difference between compressed length and original length of concrete at the top layer. By adopting the deflection shape function in Eq. (9.4), the curvature of concrete core can be obtained in Eq. (9.6).

$$K = \frac{|y'|}{(1+y'^2)^{3/2}} \approx 8Y/L^2 \tag{9.6}$$

Therefore, ΔL_C and ΔL_S can be obtained as

$$\Delta L_C = K(L - 2t_c/\tan\theta)t_2;\ \Delta L_S = \frac{1}{2}\int_0^L \left(\frac{dy}{dx}\right)^2 dx = \frac{8Y^2}{3L} \tag{9.7}$$

From above equations, the neutral axis is determined as

$$t_n = \frac{t_c}{2} + \frac{Y\xi}{6} \tag{9.8}$$

where $\xi = L\big/\left(L - 2t_c\big/\tan\theta\right)$. The value of θ normally ranges from 26.6° to 45°. In this study, θ is taken as 26.6° in accordance with Eurocode 2 (2004). Therefore, the axial strain above the neutral axis is obtained as

$$\varepsilon = \frac{8}{L^2}\left[\left(t - \frac{t_c}{2}\right)Y - \frac{Y^2\xi}{6}\right] \tag{9.9}$$

Figure 9.9 presents the comparison of the normal strain–mid-span displacement curves obtained from FE analysis and Eq. (9.9). The details of the FE model are listed in Table 9.2. It can be seen that the analytical-predicted strain agrees well with the FE-prediction. Hence, the established strain formula in Eq. (9.9) is reasonable and can be used for calculating the internal energy of concrete core.

Since it is complex to obtain the internal energy of concrete core based on current neutral axis which varies with the mid-span displacement, a constant neutral axis is proposed, based on which the equivalent curvature is then derived. If the internal energy of concrete core keeps increasing with the mid-span displacement rising from 0 to Y_n, the neutral axis t_n in Eq. (9.8) ranges from $t_c\big/2$ to $t_c\big/2 + Y_n\xi\big/6$. Therefore, it is rational to take the average neutral axis $t_c\big/2 + Y_n\xi\big/12$ as the constant neutral axis. Y_n is the minimum value of the maximum mid-span displacement (Y_{max}) and

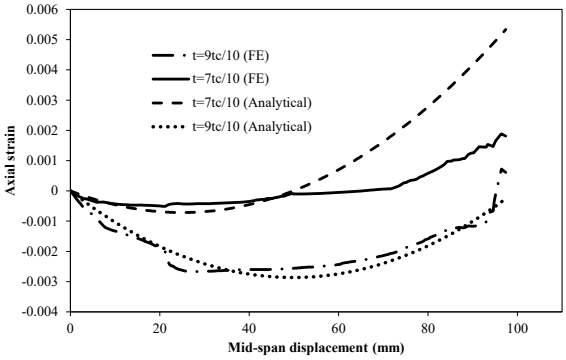

Fig. 9.9 Comparison of axial strain–displacement curves between analytical and FE prediction, reprinted from Wang et al. (2015), copyright 2022, with permission from Elsevier

Table 9.2 Details of FE model for implicit analysis on SCS sandwich panel

Front/back/end plate thickness (mm)	Concrete core thickness (mm)	Span (mm)	Steel yield stress (MPa)	Steel hardening coefficient (%)	Concrete compressive strength (MPa)
3	50	1180	320	0.5	35

Y_m. Y_m is a value of the mid-span displacement. When the mid-span displacement exceeds Y_m, the equivalent curvature starts to decrease with the increasing of mid-span displacement. Y_m will be given later after establishing the equivalent curvature.

The equivalent curvature (K_e) is derived based on the criteria that the internal energy of concrete core calculated by using original and equivalent strain expression is the same in the elastic range. The internal energy of concrete core per unit area is given as

$$\overline{u} = \int_0^{\eta_m} \frac{1}{2} E\varepsilon^2 d\eta = \frac{1}{6} E K^2 \eta_m^3 \tag{9.10}$$

where η is the distance between the compressive layer and neutral axis, and $\eta_m = T/2 - Y_n\xi/12$. Then, the equivalent curvature is obtained as

$$K_e = \frac{8Y}{L^2}\left(\frac{1 - Y\xi/3t_c}{1 - Y_n\xi/6t_c}\right)^{3/2} \tag{9.11}$$

and the strain can be expressed as

$$\varepsilon = K_e\eta = \frac{8Y\eta}{L^2}\left(\frac{1 - Y\xi/3t_c}{1 - Y_n\xi/6t_c}\right)^{3/2} \quad \left(0 \le \eta \le \tfrac{t_c}{2} - \tfrac{Y_n\xi}{12}\right) \tag{9.12}$$

Differentiating the equivalent curvature K_e with respect to mid-span displacement Y and setting it to zero leads to the solution of Y_m to be $6t_c/5\xi$. It indicates that when the mid-span displacement exceeds Y_m, the equivalent curvature K_e starts to decrease with increasing mid-span displacement.

The stress–strain curve of concrete under uniaxial compression is given by Eurocode 2 (2004) as

$$\frac{\sigma_c}{f_{cm}} = \frac{k\varepsilon/\varepsilon_o - (\varepsilon/\varepsilon_o)^2}{1 + (k-2)\varepsilon/\varepsilon_o} \quad for\ |\varepsilon| < |\varepsilon_c| \tag{9.13}$$

where k, f_{cm}, ε_o and ε_c can be found in Eurocode 2 (2004).

When all the compressive strains above the neutral axis are smaller than the crush strain of concrete ε_c, the stress–strain relationship given in Eq. (9.13) can be used for all the compressive concrete above the neutral axis. Hence, the internal energy of concrete core per unit volume can be calculated as

$$u_c(\varepsilon) = \int_0^{\varepsilon} \sigma_c d\varepsilon' = \int_0^{\varepsilon} f_{cm} \frac{k\varepsilon/\varepsilon_o - (\varepsilon/\varepsilon_o)^2}{1 + (k-2)\varepsilon/\varepsilon_o} d\varepsilon' = \varepsilon_0 f_{cm} g_1\left(\frac{\varepsilon}{\varepsilon_o}\right) \tag{9.14}$$

where $g_1(\frac{\varepsilon}{\varepsilon_o}) = \left[\frac{(k-1)^2\varepsilon/\varepsilon_o}{(k-2)^2} - \frac{(\varepsilon/\varepsilon_o)^2}{2(k-2)} - \frac{(k-1)^2\ln((k-2)\varepsilon/\varepsilon_o+1)}{(k-2)^3}\right]$.

Provided that the internal energy density of concrete core along the compression strut is the same, the internal energy of concrete core in SCS sandwich panel can be calculated as

$$U_c^u = L_e B \int_0^{\eta_m} u_c(K_e\eta) d\eta \tag{9.15}$$

where B is the width of concrete core, L_e is the length of compression strut and can be calculated as $L_e = L + 2t_c\left(1/\sin\theta - 1/\tan\theta\right)$, $g_2(\frac{K_e\eta_m}{\varepsilon_o}) = \overline{A}\left(\frac{K_e\eta_m}{\varepsilon_o}\right)^2 - \overline{B}\left(\frac{K_e\eta_m}{\varepsilon_o}\right)^3 - \overline{C}\frac{K_e\eta_m}{\varepsilon_o}\left\{\ln\left[(k-2)\frac{K_e\eta_m}{\varepsilon_o}+1\right]-1\right\} - \overline{D}\ln\left[(k-2)\frac{K_e\eta_m}{\varepsilon_o}+1\right]$, where $\overline{A} = \frac{(k-1)^2}{2(k-2)^2}$, $\overline{B} = \frac{1}{6(k-2)}$, $\overline{C} = \frac{(k-1)^2}{(k-2)^3}$, $\overline{D} = \frac{(k-1)^2}{(k-2)^4}$.

Thus, differentiating the internal energy of concrete core with respect to mid-span displacement leads to

$$\begin{aligned}\frac{dU_c^u}{dY} = \frac{L_e B\varepsilon_o^2 f_{cm}}{K_e}K_e'\Bigg\{&-g_2(\frac{K_e\eta_m}{\varepsilon_o})\frac{1}{K_e} + 2\overline{A}\left(\frac{\eta_m}{\varepsilon_o}\right)^2 K_e \\ &- 3\overline{B}\left(\frac{\eta_m}{\varepsilon_o}\right)^3 K_e^2 - \overline{C}\frac{\eta_m}{\varepsilon_o}\left[\ln\left[(k-2)\frac{K_e\eta_m}{\varepsilon_o}+1\right]-1\right] \\ &- \overline{C}\frac{k-2}{(k-2)K_e\eta_m/\varepsilon_o+1}\frac{K_e\eta_m^2}{\varepsilon_o^2} - \overline{D}\frac{k-2}{(k-2)K_e\eta_m/\varepsilon_o+1}\frac{\eta_m}{\varepsilon_o}\Bigg\}\end{aligned} \tag{9.16}$$

where $K_e' = \frac{dK_e}{dY}$. Then, the resistance–deflection function contributed by concrete core without crushing can be obtained as

$$R_{c1}(Y) = \frac{dU_c^u}{dY}\frac{1}{BLK_L} \tag{9.17}$$

where K_L is the load factor and can be calculated based on the given deflection shape function in Eq. (9.4).

When the maximum compressive strain in the concrete core exceeds crush strain of concrete ε_c, the internal energy of concrete core can be divided into two parts, i.e., the one with crushing and the rest without crushing. The internal energy of concrete core without crushing can be calculated as

$$U_{c,1} = L_e B\int_0^{\eta_0} u_c(K_e\eta)d\eta = \frac{L_e B\varepsilon_o^2 f_{cm}}{K_e}g_2(\frac{K_e\eta_0}{\varepsilon_o}) \tag{9.18}$$

where $\eta_0 = \frac{\varepsilon_c L^2}{8Y}\left(\frac{1-Y_n\xi/6t_c}{1-Y\xi/3t_c}\right)$, which is calculated by setting the strain expression in Eq. (9.12) to crushing strain ε_c. The internal energy of concrete core with crushing can be calculated as

$$U_{c,2} = L_e B(\eta_m - \eta_0)\varepsilon_o f_{cm} g_1\left(\frac{\varepsilon_c}{\varepsilon_o}\right) \tag{9.19}$$

Hence, the total internal energy of concrete core after crushing is given as

$$U_c^c = U_{c,1} + U_{c,2} \tag{9.20}$$

Similarly, differentiating the internal energy of concrete core with respect to mid-span displacement leads to

$$\frac{dU_c^c}{dY} = -\frac{L_e B\varepsilon_o^2 f_{cm}}{K_e^2} K_e' g_2\left(\frac{\varepsilon_c}{\varepsilon_o}\right) - L_e B\varepsilon_o f_{cm} g_1\left(\frac{\varepsilon_c}{\varepsilon_o}\right)\eta_0' \tag{9.21}$$

where $\eta_0' = \frac{\varepsilon_c L^2}{8}\left(1 - \frac{Y_n\xi}{6t_c}\right)^{3/2}\left[-\frac{1}{Y^2(1-Y\xi/3t_c)^{3/2}} + \frac{\xi}{2t_c Y(1-Y\xi/3t_c)^{5/2}}\right]$.

In the same way, the resistance–deflection function contributed by concrete core after crushing can be obtained as

$$R_{c2}(Y) = \frac{dU_c^c}{dY}\frac{1}{BLK_L} \tag{9.22}$$

The procedure for calculating the resistance–deflection function of the SCS sandwich panel contributed by concrete core can be summarized as follow.

Calculating the maximum strain of concrete core by Eq. (9.23).

$$\varepsilon_{\max} = \frac{8Y_m}{L^2}\left(\frac{1 - Y_m\xi/3t_c}{1 - Y_n\xi/6t_c}\right)^{3/2}\left(\frac{t_c}{2} - \frac{Y_n\xi}{12}\right) \tag{9.23}$$

For $\varepsilon_{\max} \le \varepsilon_c$, there is no concrete crushing. Then, the resistance–deflection function is given as

$$R_c = \begin{cases} R_{c1} & (Y \le Y_m) \\ 0 & (Y > Y_m) \end{cases} \tag{9.24}$$

For $\varepsilon_{\max} > \varepsilon_c$, calculating Y_0 by solving the Eq. (9.25).

$$\frac{8Y}{L^2}\left(\frac{1 - Y\xi/3t_c}{1 - Y_n\xi/6t_c}\right)^{3/2}\left(\frac{t_c}{2} - \frac{Y_n\xi}{12}\right) = \varepsilon_c \tag{9.25}$$

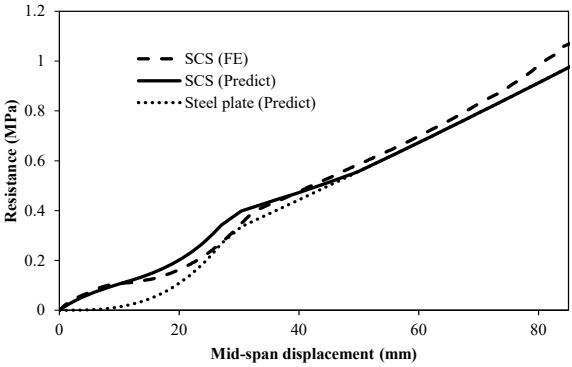

Fig. 9.10 Comparison of resistance–deflection curves between analytical and FE models, reprinted from Wang et al. (2015), copyright 2022, with permission from Elsevier

Then, the resistance–deflection function is given as

$$R_c = \begin{cases} R_{c1} \ \ (Y \le Y_0) \\ R_{c2} \ \ (Y_0 < Y \le Y_m) \\ 0 \ \ (Y > Y_m) \end{cases} \tag{9.26}$$

The total resistance of the SCS sandwich panel is obtained by summing the resistances contributed by steel plates and concrete core. Figure 9.10 presents the comparison of the analytical-predicted resistance–deflection of the SCS sandwich panel with that obtained by FE analysis, and good agreement between them can be observed. The resistance of steel plates is also plotted in Fig. 9.10, and it is lower than the resistance of the SCS sandwich panel obtained from FE analysis, especially for small displacement. This indicates that the concrete core helps in improving the initial stiffness of axially-restrained SCS sandwich panel, whereas the steel plates absorb the majority of blast energy when the SCS sandwich panel experiences large deformation.

9.3.2 DIF for SDOF Model

The strain rate effect is generally included in the analytical model by means of DIF which can be defined as a function of strain rate. In the FE method, the DIF–strain rate relationship can be directly specified in the constitutive model, and the varying value of DIF depending on strain rate can be applied in the FE calculation (Hallquist 2006). For the SDOF method, a constant DIF value is generally adopted to scale either the yield strength, ultimate strength or both of them depending on the deformation mode (UFC 2008; ASCE 2011). It has been argued that a single DIF value might not accurately capture the strain rate effect for highly varying strain rate, and it could be too conservative for large plastic deformation cases. Therefore, varying DIF in terms of strain rate is introduced into the SDOF and Lagrange Equation models to

accurately capture the strain rate effect. Since the strain rate has little effect on the Young's modulus of steel, it can be kept unchanged during calculation, while both yield stress and yield strain vary with the strain rate.

9.3.2.1 DIF for Steel Plate

The varying DIF can be taken into consideration during transformation of actual structural member to its equivalent SDOF system through energy balance principle. The variation for the internal energy of steel plates and its equivalent SDOF system is given by Eqs. (9.27) and (9.28), respectively.

$$dU_a = \int_0^L f(\dot{\varepsilon}_p)\sigma(Y)Ad\varepsilon dx \tag{9.27}$$

$$dU_e = DIF_s * K_R * R(Y)dY = DIF_s * \int_0^L \sigma(Y)Ad\varepsilon dx \tag{9.28}$$

where K_R is the resistance factor. By assuming that the internal energy along the span is constant and equating the above two equations leads to

$$DIF_s = \frac{\int_0^L f(\dot{\varepsilon}_p)dx}{L} \tag{9.29}$$

The configuration of infinitesimal element (dx) is shown in Fig. 9.11 at t and $t + \Delta t$, based on which the plastic strain rate can be obtained as

$$\dot{\varepsilon}_p = \frac{[\phi(x)]^2 Y\dot{Y}}{1 + [\phi(x)Y]^2} \tag{9.30}$$

Equation (9.30) defines the strain rate in terms of shape function, displacement and velocity. For steel material, Eq. (9.31) can be obtained by using the Cowper-Symonds model to define the DIF as a function of strain rate.

$$f(\dot{\varepsilon}_p) = 1 + \left(\frac{[\phi(x)]^2 \dot{Y}Y}{c + c[\phi(x)Y]^2}\right)^{1/p} \tag{9.31}$$

Substituting Eq. (9.31) and shape function in Eq. (9.4) into Eq. (9.29), the DIF_s can be calculated as

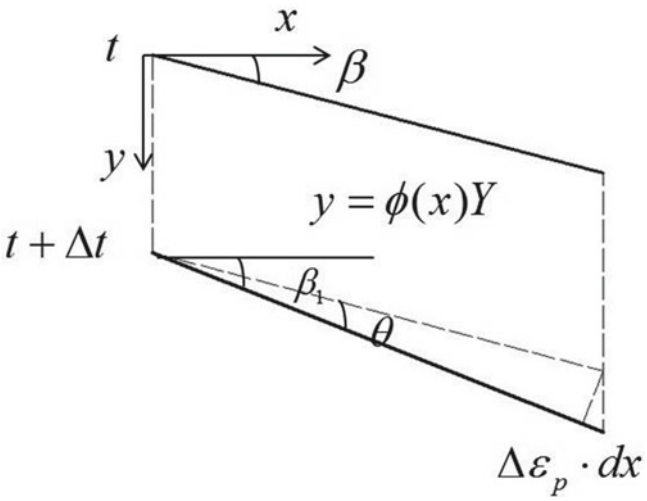

Fig. 9.11 Configuration of infinitesimal element along span, reprinted from Wang et al. (2015), copyright 2022, with permission from Elsevier

$$DIF_{\mathrm{s}} = 1 + \frac{\int_0^L \left(\frac{\chi \dot{\chi}}{c\chi^2 + c/16(1-2x/L)^2} \right)^{1/p} dx}{L} \tag{9.32}$$

where $\chi = Y/L$ is the mid-span displacement to span ratio.

9.3.2.2 DIF for Concrete Core

The energy balance principle is also adopted to obtain the DIF for concrete core. The variation for the internal energy of concrete core without considering strain rate effect is given as

$$dU_c = BL_e f_{cm} \int_0^{\eta_m} \frac{kK_e\eta/\varepsilon_0 - (K_e\eta/\varepsilon_0)^2}{1 + (k-2)K_e\eta/\varepsilon_0} \eta d\eta dK_e \tag{9.33}$$

Then, we have

$$\frac{dU_c}{dY} = BL_e f_{cm} \int_0^{\eta_m} \frac{kK_e\eta/\varepsilon_0 - (K_e\eta/\varepsilon_0)^2}{1 + (k-2)K_e\eta/\varepsilon_0} \eta d\eta \frac{dK_e}{dY} \tag{9.34}$$

In the same way, the following equation can be obtained by considering the strain rate effect.

$$\frac{dU_{cD}}{dY} = BL_e f_{cm} \int_0^{\eta_m} D_c(\eta \dot{K}_e) \frac{kK_e\eta/\varepsilon_0 - \left(K_e\eta/\varepsilon_0\right)^2}{1+(k-2)K_e\eta/\varepsilon_0} \eta d\eta \frac{dK_e}{dY} \tag{9.35}$$

Therefore, the DIF for concrete core is obtained as

$$DIF_{c1} = \frac{\int_0^{\eta_m} D_c(\eta \dot{K}_e) \frac{kK_e\eta/\varepsilon_0 - (K_e\eta/\varepsilon_0)^2}{1+(k-2)K_e\eta/\varepsilon_0} \eta d\eta}{\int_0^{\eta_m} \frac{kK_e\eta/\varepsilon_0 - (K_e\eta/\varepsilon_0)^2}{1+(k-2)K_e\eta/\varepsilon_0} \eta d\eta} \tag{9.36}$$

Equation (9.36) is only used to scale up the R_{c1}, and the DIF for scaling up R_{c2} is given in Eq. (9.37).

$$DIF_{c2} = \frac{\int_0^{\eta_0} D_c(\eta \dot{K}_e) \frac{kK_e\eta/\varepsilon_0 - (K_e\eta/\varepsilon_0)^2}{1+(k-2)K_e\eta/\varepsilon_0} \eta d\eta}{\int_0^{\eta_0} \frac{kK_e\eta/\varepsilon_0 - (K_e\eta/\varepsilon_0)^2}{1+(k-2)K_e\eta/\varepsilon_0} \eta d\eta} \tag{9.37}$$

In above equations, $D_c(\dot{\varepsilon})$ defines the relationship between DIF and strain rate of concrete core and is given by CEB-FIP (1993).

$$D_c(\dot{\varepsilon}) = \begin{cases} \left(\dot{\varepsilon}/\dot{\varepsilon}_s\right)^{1.026\delta_s} & (\dot{\varepsilon} \le 30s^{-1}) \\ \beta_s\left(\dot{\varepsilon}/\dot{\varepsilon}_s\right)^{1/3} & (\dot{\varepsilon} > 30s^{-1}) \end{cases} \tag{9.38}$$

where $\delta_s = 1/(5+9f_{cm}/10)$, $\beta_s = 10^{(6.156\delta_s - 2.0)}$ and the static strain rate $\dot{\varepsilon}_s = 30 \times 10^{-6}$.

9.3.3 Equation of Motion for SDOF System

The equation of motion for the SDOF system can be established as

$$K_{LM}[\rho_s(t_{s1}+t_{s2}) + \rho_c t_c]\ddot{Y} + R_{s1} + R_{s2} + R_c = P(t) \tag{9.39}$$

where ρ_s and ρ_c are densities of steel and concrete; t_{s1}, t_{s2} and t_c are thicknesses of front steel plate, back steel plate and concrete core; R_{s1}, R_{s2} and R_c are the resistances of the SCS sandwich panel contributed by the front steel plate, back steel plate and concrete core; $P(t)$ is pressure–time history of blast loading.

It should be noted that the equation of motion in Eq. (9.39) is only valid before the separation of front steel plate. The SCS sandwich panel can be divided into two parts, i.e., front steel plate and concrete core + back steel plate. Since the resistance intensity (i.e., $R_i \big/ \rho_i t_i$) of the steel plate is higher than that of concrete core for large deformation, the front steel plate may separate from concrete core when the velocity reduction rate of the front steel plate is higher than that of concrete core and back steel plate. Therefore, the front steel plate starts to separate from concrete core when $[R_{s1} - P(t)] \big/ \rho_s t_{s1} > (R_{s2} + R_c) \big/ (\rho_s t_{s2} + \rho_c t_c)$ and the equation of motion changes to

$$K_{LM}(\rho_s t_{s2} + \rho_c t_c)\ddot{Y} + R_{s2} + R_c = 0 \tag{9.40}$$

The fourth-order Runge–Kutta time stepping procedure is utilized to solve the equations of motion in Eqs. (9.39) and (9.40).

9.4 Lagrange Equation Model

9.4.1 Equation of Motion

According to the Lagrange Equation model, the equations of motion can be formulated as

$$\frac{d}{dt}\left(\frac{\partial T}{\partial \dot{C}_i}\right) + \frac{\partial (U+V)}{\partial C_i} = 0, \quad i = 1, 2, ..., n. \tag{9.41}$$

where T is the kinetic energy, U is the internal energy, V is the potential energy of loading and C_i is the generalized displacement.

For the front and back steel plate in the SCS sandwich panel, only the tensile membrane force is considered to resist blast loading, T, U and V in Eq. (9.41) can be formulated in Eqs. (9.42), (9.44) and (9.45), respectively.

$$T = \frac{1}{2}\int_0^L \rho A \dot{w}^2 dx \tag{9.42}$$

where L is the span, ρ is the density, A is the cross-section area, and $\dot{w}$ is the velocity of the steel plate. The deflection of the steel plate, w, with n generalized displacements and deflection shape functions are given as

$$w(x,t) = \sum_{i=1}^{n} C_i(t)\phi_i(x) \tag{9.43}$$

The internal energy of steel plate U_s is calculated as

$$U_s = \begin{cases} \frac{1}{2} EA \frac{\Delta L^2}{L}, & \Delta L \le \Delta L_y \\ \frac{EA}{2L}\left[\alpha \Delta L^2 + 2(1-\alpha)\Delta L_y \Delta L + (\alpha - 1)\Delta L_y^2\right], & \Delta L > \Delta L_y \end{cases} \tag{9.44}$$

where ΔL is the difference between the developed length and original length of the steel plate. For potential energy,

$$V = -\int_0^L P(t) w(x,t) dx \tag{9.45}$$

It should be noted that front steel plate must be removed after it separating from concrete core during calculation, similar to the SDOF model.

For the concrete core in the SCS sandwich panel, the calculation of kinetic energy T and potential energy V is same with the front and back steel plates. However, the derivation of the internal energy of concrete core U_c and its differential with generalized displacements in Eq. (9.41) are complex. To avoid recalculating the internal energy of concrete core, it is assumed that the combined deflection shape function in the Lagrange Equation model is same with that in the SDOF model. This assumption is reasonable for the axially-restrained SCS sandwich panel under blast loading, since the deflection shape function has little effect on the structural response, and the internal energy of concrete core is relatively small compared with steel plates, especially for the large deflection.

The mid-span displacement of the SCS sandwich panel is expressed as

$$Y = \sum_{i=1}^{n} C_i(t) \phi_i(L/2) \tag{9.46}$$

Hence, the differential of the internal energy of concrete core U_c with respect to generalized displacement C_i can be obtained as

$$\frac{\partial U_c}{\partial C_i} = \frac{\partial U_c}{\partial Y} \frac{\partial Y}{\partial C_i} \tag{9.47}$$

9.4.2 DIF for Lagrange Equation Model

The DIF for concrete core in the Lagrange Equation model is same with that in the SDOF method, since the same deflection shape function is assumed when calculating

the internal energy of concrete core. However, the DIF for steel plates should be recalculated, as the different combined deflection shape function is employed for the Lagrange Equation model. The energy balance principle is utilized to introduce the varying DIF into the Lagrange Equation model. By applying the differential operator on the internal energy with and without consideration of strain rate effect (i.e., U_s and U_{sD}) for the front and back steel plates, the following equations are obtained

$$dU_s = \tilde{V}\sigma d\varepsilon \tag{9.48}$$

$$dU_{sD} = \tilde{V} f\left(\dot{\varepsilon}_p\right)\sigma d\varepsilon = f\left(\dot{\varepsilon}_p\right)dU_s \tag{9.49}$$

where $\tilde{V}$ is the volume of the steel plate. Equation (9.49) can be rewritten as

$$\sum_{i=1}^{n}\left(\frac{\partial U_{sD}}{\partial C_i} - f(\dot{\varepsilon}_p)\frac{\partial U_s}{\partial C_i}\right)dC_i = 0 \tag{9.50}$$

Setting $\frac{\partial U_{sD}}{\partial C_i} = f(\dot{\varepsilon}_p)\frac{\partial U_s}{\partial C_i}$ $(i = 1,2,\ldots,n)$ satisfies Eq. (9.50) and substituting them into Eq. (9.41) gives the equations of motion with varying DIF being considered.

Since the elongation of the steel plate ΔL is a function of C_1, C_2, …, C_n, i.e., $\Delta L = g(C_1, C_2, ..., C_n)$, the strain rate can be derived as

$$\dot{\varepsilon} = \frac{\Delta\dot{L}}{L} = \frac{1}{L}\left(\frac{\partial g}{\partial C_1}\dot{C}_1 + \frac{\partial g}{\partial C_2}\dot{C}_2 + ... + \frac{\partial g}{\partial C_n}\dot{C}_n\right) \tag{9.51}$$

By adopting the Cowper-Symonds model to establish the relationship between strain rate and DIF, the following equation is obtained.

$$\frac{\partial U_{sD}}{\partial C_i} = \left[1 + \left(\frac{\dot{\varepsilon}}{c}\right)^{1/p}\right]\frac{\partial U}{\partial C_i} \tag{9.52}$$

9.5 Results and Discussions

In this section, the FE model is adopted to simulate the axially-restrained SCS sandwich panel subjected to blast loading, and the results are compared with the predictions from analytical models. Since the maximum displacement instead of the displacement–time history is the most concern in the blast resistant design, the maximum displacements of SCS sandwich panels under blast load (a triangular blast pressure profile with zero rise time) are obtained using FE and analytical models and summarized in Table 9.3. The displacement of the SCS sandwich panel is given in Eq. (9.53) by employing combined deflection shape functions.

Table 9.3 Maximum displacement comparison

t_{s1}	t_{s2}	t_c	L	$P_{\max}$	t_d	Max dis (mm)				Error (%)		
						FE	SDOF	LEM1	LEM2	SDOF	LEM1	LEM2
3	3	70	1180	10	0.5	55.7	61.3	63.1	60.1	9.96	13.13	7.87
				1	5	46.8	52.8	53.9	51.6	12.92	15.33	10.39
				0.5	5000	51.8	63.6	56.8	54.7	22.69	9.60	5.52
3	3	50	1180	10	0.5	66.8	71.2	76.9	73.5	6.56	18.09	10.07
				1	5	55.5	61.3	63.8	61.6	10.36	18.85	10.93
				0.5	5000	56.6	66.2	61.4	58.9	16.97	13.04	4.07
1.5	3	50	1180	10	0.5	72.1	75.9	82.8	79.0	5.37	17.71	9.65
				1	5	61.0	67.9	71.5	68.9	11.25	21.01	12.81
				0.5	5000	68.1	82.9	75.3	71.5	21.79	14.91	4.95
1.5	1.5	50	1180	5	0.5	53.8	54.2	57.3	54.1	0.68	8.77	0.39
				0.5	5	46.7	50.0	50.5	47.9	7.08	10.92	2.68
				0.25	5000	56.3	64.4	58.5	56.1	14.31	8.44	-0.36

Note the unit of t_{s1}, t_{s2}, t_c and L is mm; the units of $P_{\max}$ and t_d are MPa and ms; LEM1 and LEM2 stands for Lagrange Equation model with $a = 1$, $b = 2$ and $a = 2$, $b = 3$, respectively

$$w(x,t) = C_1(t)\left[\frac{4}{L^2}(Lx - x^2)\right]^a + C_2(t)\left[\frac{4}{L^2}(Lx - x^2)\right]^b \tag{9.53}$$

where the term in the bracket is the deflection shape function defined in the SDOF model, and the parameters a and b are specified with different values to represent different deflection shape functions. It should be mentioned that any reasonable combination of deflection shape functions is acceptable, and more number of deflection shape functions may provide more accurate predictions.

Table 9.3 shows that the analytical-predicted maximum displacements of SCS sandwich panels match well with the FE predictions. However, the slightly larger values of maximum displacement are observed for the analytical-predictions, which may be caused by the underestimation of internal energy and neglect of energy dissipated through friction and damping in the analytical models. Another reason may be attributed to the different deflection shape functions between the FE and analytical models.

For the predictions from the SDOF model, they exhibit better match with the FE predictions in the impulsive loading range (i.e., short loading duration), with the differences of maximum displacement between the two models less than 10%. In addition, the separation between the front steel plate and concrete core during calculation can also be well captured by the SDOF model, as shown in Fig. 9.12. However, the SDOF model provides larger values of maximum displacement than that of FE model in the quasi-static loading range. This may be caused by the neglect of

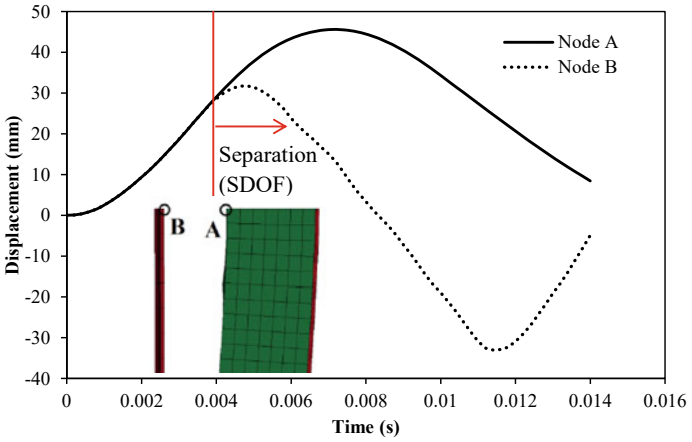

Fig. 9.12 Comparison of the separation time between FE and SDOF analysis ($t_s = 3$ mm; $t_c = 70$ mm, $P_{max} = 1$ MPa; $t_d = 5$ ms), reprinted from Wang et al. (2015), copyright 2022, with permission from Elsevier

confinement effect on compressive strength of concrete when deriving the resistance–deflection function contributed by concrete core. This effect is more significant in quasi-static loading range since the separation is not observed during calculation.

For the Lagrange Equation model, it is found that the LEM2 provides closer predictions to the FE model as compared to LEM1. The deflection shape of the SCS sandwich panel obtained from FE analysis is compared with those from SDOF and LEM2 models, as presented in Fig. 9.13. The deflection shape from LEM2 is found to be closer to that from FE model. Since two combined deflection shape functions are employed for the Lagrange Equation model and a varying deflection shape can be achieved during calculation, it can provide more accurate predictions as compared to the SDOF model with single deflection shape function. It was observed by Baker et al. (1983) that the different deflection shape functions should be employed for

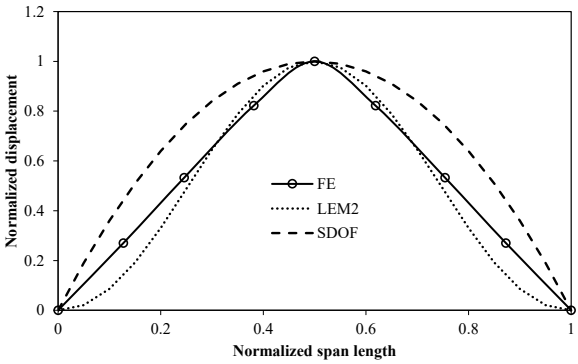

Fig. 9.13 Comparison of the deflection shape between FE and analytical model ($t_s = 3$ mm; $t_c = 70$ mm, $P_{max} = 1$ MPa; $t_d = 5$ ms), reprinted from Wang et al. (2015), copyright 2022, with permission from Elsevier

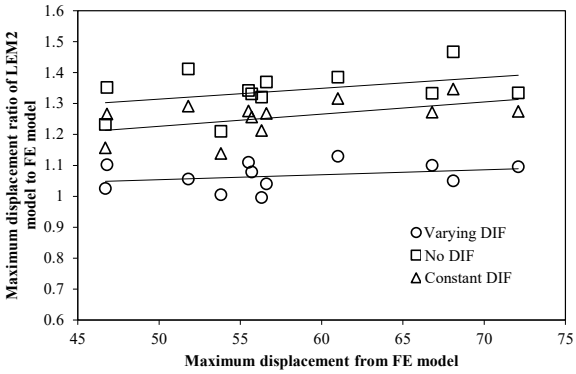

Fig. 9.14 Varying DIF effect on the maximum displacement, reprinted from Wang et al. (2015), copyright 2022, with permission from Elsevier

the SDOF model to obtain the exact solutions of simply supported beams under impulsive and quasi-static loading ranges. Therefore, the SODF model with single deflection shape function generally cannot provide accurate predictions in all the loading ranges (i.e., impulsive, dynamic and quasi-static loading ranges).

Both Lagrange Equation models and SDOF model provide better predictions with decreasing of the steel plate thickness, which indicates that the internal energy of steel plate is underestimated. This underestimation may be caused by the assumed deflection shape functions and the assumption that the strain is uniformly distributed along the span. The effect of varying DIF on the maximum displacement of the SCS sandwich panel is presented in Fig. 9.14. The LEM2 with varying DIF, constant DIF and without DIF was adopted to compare with the FE analyses. The constant DIF values of steel and concrete are adopted as 1.10 and 1.12, respectively (ASCE 2011). Figure 9.14 shows that the LEM2 with varying DIF provides better predictions than the LEM2 with constant DIF or without DIF. It is also observed from the fitting curves that the LEM2 with varying DIF provides approximately constant differences between the LEM2 and FE model, while the differences of LEM2 with constant DIF or without DIF exhibits increase with increasing maximum displacement. This demonstrates that the proposed varying DIF can more accurately capture the strain rate effect regardless of the maximum displacement, whereas the LEM2 with constant DIF or without DIF may overestimate the responses, especially for the large defection.

For the axially-restrained non-composite SCS sandwich panels, the separation of front steel plate and concrete core generally occurs under impulsive loading range. Therefore, it is more efficient to improve the blast resistance by enhancing the back steel plate instead of front steel plate. Moreover, increasing the thickness of concrete core is also an important way, since it can reduce the obtained kinetic energy under blast loading.

9.6 Summary

Two analytical models were developed to predict the responses of axially-restrained SCS sandwich panels subjected to blast loading. The force equilibrium equation was employed to derive the resistance–deflection function of the SCS sandwich panel contributed by steel plates. The energy balance principle was adopted to obtain the resistance–deflection function contributed by concrete core. The varying DIF in terms of strain rate was included in the two analytical models, which could accurately capture the strain rate effect. The FE analyses were employed to validate the proposed two analytical models. Through the comparison of maximum displacements obtained from FE and analytical models, the analytical models were found to reasonably predict the responses of axially-restrained SCS sandwich panels under blast loading. It was observed from both FE and analytical models that the front steel plate was prone to separate from the concrete core owing to the absence of shear connectors. Hence, enhancing the back steel plate was preferred to improve blast resistance of the axially-restrained non-composite SCS sandwich panel.

References

ASCE/SEI 59-11 (2011) Blast protection of buildings. American Society of Civil Engineers, Reston, Virginia

Bailey CG (2001) Membrane action of unrestrained lightly reinforced concrete slabs at large displacements. Eng Struct 23:470–483

Baker WE, Cox PA, Westine PS et al (1983) Explosion and hazards and evaluation. Elsevier Scientific Publishing Compay, Amsterdam

Biggs JM (1964) Introduction to structural dynamics. McGraw-Hill, New York

Carta G, Stochino F (2013) Theoretical models to predict the flexural failure of reinforced concrete beams under blast loads. Eng Struct 49:306–315

CEB-FIP (1993) CEB–FIP model code 1990. Redwood Books, Wiltshire

Cowper GR, Symonds PS (1958) Strain hardening and strain rate effects in the impact loading of cantilever beams. Applied Mathematics Report, Brown University

Donaldson BK (2006) Introduction to structural dynamics. Cambridge University Press, New York

Eurocode 2 (2004) Design of concrete structures – Part 1–1: General rules and rules for buildings. BS EN 1992–1–1, London

Federal Highway Administration (2007a) Evaluation of LS-DYNA concrete material model 159

Federal Highway Administration (2007b) Users manual for LS-DYNA concrete material model 159

Hallquist JO (2006) LS-DYNA theory manual. Livermore Software Technology Corporation (LSTC). Livermore, California

Jones J, Wu C, Oehlers DJ et al (2009) Finite difference analysis of simply supported RC slabs for blast loadings. Eng Struct 31:2825–2832

Jones N (1988) Structural impact. Cambridge University Press, NewYork

Kang KW, Lee SC, Liew JYR (2013) Analysis of steel–concrete composite column subject to blast. P I Civil Eng–Str B 166:15–27

Lan S, Lok TS, Heng L (2005) Composite structural panels subjected to explosive loading. Constr Build Mater 19:387–395

Langdon GS, Schleyer GK (2005) Inelastic deformation and failure of profiled stainless steel blast wall panels. Part II: analytical modelling considerations. Int J Impact Eng 31:371–399
Li GQ, Guo SX, Zhou HS (2007) Modeling of membrane action in floor slabs subjected to fire. Eng Struct 29:880–887
Liew JYR, Sohel KMA (2009) Lightweight steel–concrete–steel sandwich system with J–hook connectors. Eng Struct 31(5):1166–1178
Liew JYR, Sohel KMA, Koh et al (2009) Impact tests on steel–concrete–steel sandwich beams with lightweight concrete core. Eng Struct 31(9):2045–2059
Liew JYR, Wang TY (2011) Novel steel–concrete–steel sandwich composite plates subjected to impact and blast load. Adv Struct Eng 14(4):673–686
Nassr AA, Razaqpur AG, Tait MJ et al (2012) Single and multi-degree of freedom analysis of steel beams under blast loading. Nucl Eng Des 242:63–77
Remennikov AM, Kong SY (2012) Numerical simulation and validation of impact response of axially–restrained steel–concrete–steel sandwich panels. Compo Struct 94:3546–3555
Remennikov AM, Kong SY, Uy B (2013) The response of axially restrained non–composite steel–concrete–steel sandwich panels due to large impact loading. Eng Struct 49:806–818
Schleyer GK, Hsu SS (2000) A modelling scheme for predicting the response of elastic–plastic structures to pulse pressure loading. Int J Impact Eng 24:759–777
UFC 3–340–02 (2008) Structures to resist the effects of accidental explosions. US Department of Army, Navy and the Air Force, Washington, DC
Wang Y, Liew JYR, Lee SC (2015) Theoretical models for axially restrained steel–concrete–steel sandwich panels under blast loading. Int J Impact Eng 76:221–231
Wang Y, Xiong MX (2015) Analysis of axially restrained water storage tank under blast loading. Int J Impact Eng 86:167–178